

Isothermal shocks in Abell 2199 and 2A 0335+096?

J.S. Sanders^{*} and A.C. Fabian

Institute of Astronomy, Madingley Road, Cambridge. CB3 0HA

7 February 2020

ABSTRACT

We report on a partially circular X-ray surface brightness discontinuity found at about 55 kpc from the centre of Abell 2199 with *Chandra X-ray observatory* observations. Unlike cold fronts found in other clusters, the feature shows no temperature change across it but has an apparent density jump. We therefore identify it as a weak isothermal shock associated with the central AGN and the inflation of its radio bubbles, as found in the Perseus cluster. We examine a similar feature at 40 kpc radius found by Mazzotta et al in 2A 0335+096, and conclude that it too is an isothermal shock. The change in density across these shocks implies a Mach number of 1.5. The implication of this discovery is that such shocks are common in clusters of galaxies, and are an important mechanism for the transport of energy from a central supermassive black hole into the cluster core.

Key words: X-rays: galaxies — galaxies: clusters: individual: Abell 2199 — galaxies: clusters: individual: 2A 0335+096 — intergalactic medium — cooling flows

1 INTRODUCTION

Abell 2199 is a regular, rich, X-ray bright cluster of galaxies at a redshift of 0.0309. The X-ray emission is steeply peaked (Peres et al 2001). *Chandra* X-ray observations of the cluster show that it is regular near the centre, although there is more bright X-ray emission to the south where the older parts of the radio source lie (Johnstone et al 2002). Abell 2199 hosts the unusual radio galaxy 3C338 which shows evidence for multiple episodes of radio emission. The extended, older emission clearly coincides with two outer large depressions 25 kpc either side of the nucleus.

2A 0335+096 is another bright, nearby ($z = 0.0349$) galaxy cluster. *Chandra* observations of the cluster found complex substructure in the core (Kawano, Ohto & Fukazawa 2003; Mazzotta, Edge & Markevitch 2003), consisting of a number of X-ray bright blobs and a “cold front” 40 kpc to the south of the centre. The cold front is peculiar, showing no temperature discontinuity across it (Mazzotta et al 2003). The cluster hosts another unusual radio source (Sarazin et al 1995), and was the subject of a deep *XMM-Newton* observation (Werner et al 2006).

In this letter we examine *Chandra* observations of Abell 2199 and 2A 0335+096. We have discovered a jump in surface brightness in Abell 2199 without evidence for any temperature change across it. We identify this as an isothermal shock. We also investigate the “cold front” in 2A 0335+096, and conclude it is an isothermal shock too. Finally we examine a *Chandra* image of H 1821+643 ($z = 0.297$) and report a suggestive ring structure.

We assume $H_0 = 70 \text{ km s}^{-1} \text{ Mpc}^{-1}$ when calculating distances, so the angular scales are 0.61, 0.685 and 4.39 kpc arcsec^{−1} for Abell 2199, 2A 0335+096 and H 1821+643, respectively.

2 DATA ANALYSIS

2.1 Abell 2199

The analysis was undertaken with *Chandra* OBSIDs 498 and 497, taken with the detectors at -110°C and -120°C , respectively. These datasets used the ACIS-S array for imaging. The event files were reprocessed with CIAO 3.3.0.1, using CALDB 3.10. Light curves for the event files were extracted from the ACIS-S1 CCD in the 2.5 to 7 keV band to filter the data for flares. This CCD uses the same front-illuminated technology as the ACIS-S3 CCD, and so is a good choice for filtering for flares. This energy band is optimised for flare filtering (Markevitch 2002). We filtered out flared time periods by eye from each dataset. This yielded a total of 33.1 ks clean exposure.

For spectral fitting, background spectra were extracted from blank-sky fields, reprocessed and reprojected to match their respective foreground observations. The exposure of the background observation was adjusted to give the same count rate in the 10–12 keV band as the foreground observation. Response matrices were created using the CIAO MKRMF tool, weighting according to the number of counts between 0.5 and 7 keV in each spectral region, and ancillary response matrices were made using MKWARF.

2.2 2A 0335+096

For 2A 0335+096, we analysed the *Chandra* OBSID 919. This observation again used the ACIS-S3 CCD for imaging. We reprocessed the data in the same way as above. As was noted by Mazzotta et al (2003), most of this observation is affected by a mild flare. Using the ACIS-S1 CCD, we removed periods where the count rate was above 0.35 counts per second in the above band.

^{*} E-mail: jss@ast.cam.ac.uk

This yielded a total exposure of 11.8 ks. Using a slightly less strict time selection, Mazzotta et al (2003) noted that the cluster emission is dominant over the flare, and the inclusion of a component for the flare in the modelling makes very little difference to the results. We therefore ignore the flare in our modelling. For this observation we again made background spectra from a blank-sky observation. Responses were created using MKACISRMF.

3 RESULTS

In Fig. 1 we show an unsharp-masked image of Abell 2199. An exposure-map corrected image of the cluster was made using both datasets in the 0.5 to 6 keV band. This image was smoothed by Gaussians of 1.96 and 19.6 arcsec, and the second image was subtracted from the first. This procedure enhances features between these two scales, by subtracting the variation on larger and smaller scales. Immediately a semi-circular ring shaped feature to the south and east of the core. We also plot on the figure the 1.4 GHz radio emission. As reported by Johnstone et al (2002), the radio emission occupies holes in the X-ray emission. There are additional “fossil” radio bubbles which have no radio association, found to the south of the nucleus.

2A 0335+096 shows a similar surface brightness discontinuity to the south of its core (Fig. 2), as was noted by Mazzotta et al (2003).

We have created surface brightness profiles across these features (Fig. 3), where they are most circular in shape on the sky. In the central region of Abell 2199, the surface brightness is relatively flat. A powerlaw fit gives a slope of around -0.7. The surface brightness profile then quickly steepens, giving a slope of -1.6 at large radii. In 2A 0335+096, the central surface profile is steeper than Abell 2199, with an index of -1.8. There appears to be a surface brightness discontinuity at a radius of around 0.9 arcmin. The surface brightness then appears to decline with a similar slope to the interior, with an index of around -1.6.

We have also measured temperature profiles across these features. Using sectors with the same range of angles as the surface brightness profiles, we fitted single temperature MEKAL models to spectra extracted from annuli. In the fits the absorption, temperature, metallicity relative to solar, and normalisation were free. These resulting temperature profiles are plotted in Fig. 4. Also shown are dotted lines at the approximate radii of the discontinuities. From the emission measures we calculated deprojected electron densities in each shell, assuming spherical symmetry. Working from the outer annulus, the contribution to the emission measure from annuli external to the one being examined were subtracted, to calculate the density. Approximate pressures were calculated by multiplying the projected temperature and deprojected density.

The deprojected densities we calculated are very similar to the values produced using the PROJECT model in XSPEC, which accounts for projection. The projected temperatures show very little difference to the deprojected ones from PROJECT, but have smaller error bars. We do not find any evidence for metallicity jumps across the surface brightness changes, although the uncertainty on the abundance measurements could hide moderate changes.

4 DISCUSSION

It can be seen that the density abruptly declines outward across each of these surface brightness features. In Abell 2199 the den-

sity drops by around 40 per cent, and in 2A 0335+096 it falls by 45 per cent. However there is no significant temperature change over either edge. This means that there are discontinuities in the pressure profiles, implying that these features are not static. They are not cold-fronts (Markevitch et al 2000), which are continuous in pressure.

We therefore identify the features are isothermal shocks, as discovered in the Perseus cluster (Fabian et al 2006). Shocks may appear to be isothermal if conduction is operating efficiently. As the electrons move faster than the ions, they can travel ahead of the shock. This means that the increase in electron temperature (which we measure from the X-ray spectra) is smoothed out over a large region, while the ion temperature is discontinuous over the shock.

Using equation (10-2) of Spitzer (1978), for a non-radiating shock the pre and postshock densities, ρ_1 and ρ_2 , are related to the Mach number of shock, M , by

$$\frac{\rho_1}{\rho_2} = \frac{\gamma - 1}{\gamma + 1} + \frac{2}{(\gamma + 1)M^2}. \quad (1)$$

Using a value of the ratio of the specific heats, γ , of 5/3, this yields a Mach number, M , of around 1.5 for both shocks. If the shocks were not isothermal, this would imply a 50 per cent rises in temperature which are not observed.

A similar shock may exist in the cluster surrounding the quasar H 1821+643. In Fig. 5 we show a 99.6 ks *Chandra* Low Energy Transmission Grating (LETG) zeroth order image of the cluster. The effective area of the instrument with the the LETG in place is reduced by a factor of 6-8, so the image represents a partial, noisy, snapshot. Visible in the image is a ring around the core, roughly 10 arcsec (44 kpc) in radius. Also seen is a 5 arcsec long mushroom shaped feature to the north of the nucleus, which is spatially coincident with, and has the same morphology as its radio lobe.

As we have found isothermal shocks in three nearby cool core clusters, it appears likely that they are widespread. If this is the case, they are likely to be an important mechanism for the transport of energy from the central active nucleus to the surrounding cluster. The discovery of an isothermal shock in Perseus was completely unexpected, but they could be very important for unravelling the heating and cooling processes in clusters. In addition, their existence may indicate that the magnetic field in cluster cores may be radial, for conduction to be operating efficiently across shocks. However not all shocks are isothermal, for example the weak shocks in Cygnus A (Wilson, Smith & Young 2006) and M87 (Forman et al 2006).

We note that there is a problem for the clusters if the shocks are not isothermal, since the temperature jump should be much higher at smaller radii. The density profile of the cool cores of clusters approximately varies inversely with radius ($n \propto r^{-1}$), so a pressure driven shock has a velocity v which evolves with radius r as $v \propto r^{-1}(E/n)^{1/2}$. A jump of say 0.5 keV at radius 50 kpc would have had a shock temperature ($T \propto v^2$) of over 10 keV when at 10 kpc, which is around the size of the bubbles seen. This problem is particularly acute for the M87 shock where Forman et al (2006) report a jump of 0.5 keV at 13 kpc when the typical bubble size is 1.5 kpc. The temperature of the gas is observed to drop inward whereas a shock would predict much higher inner temperatures, even though the gas would cool somewhat by adiabatic expansion after the shock has passed.

Repeat efficient shocking of gas in cool cluster cores would soon create temperature, and entropy, profiles disagreeing markedly from the steady, inward drop, generally found (at least one third of clusters have such cool cores, Dunn et al 2005).

We have investigated several processes which could tend to

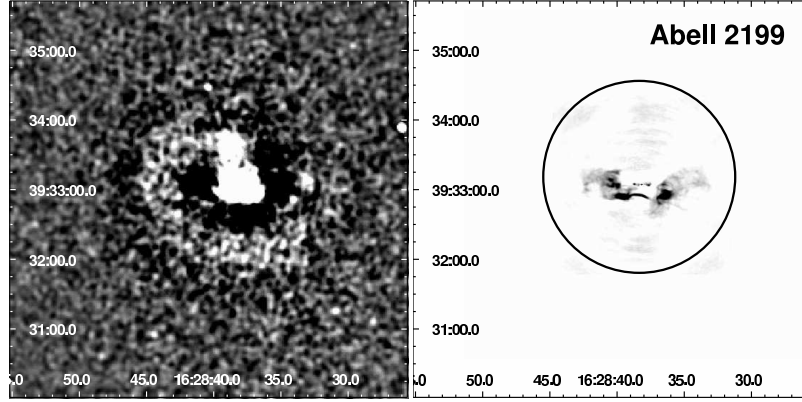


Figure 1. (Left) Unsharp-masked image of the core of Abell 2199 in the 0.5 to 6 keV band. (Right) 1.4 GHz VLA radio map of the same region (Giovannini et al 1998). The position of the X-ray edge is marked by a circle.

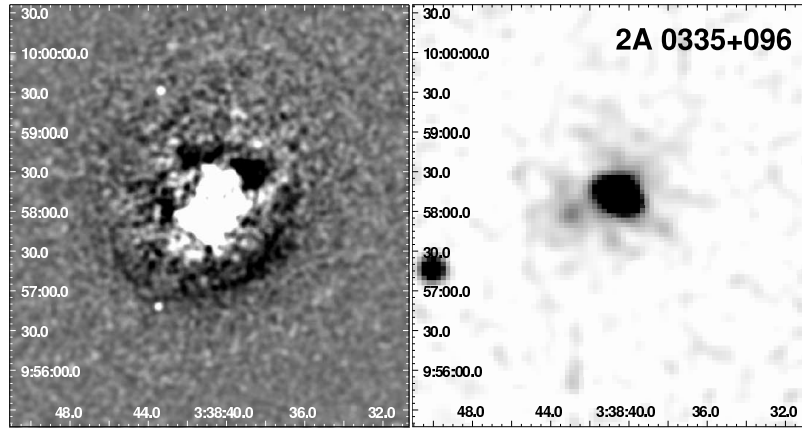


Figure 2. (Left) Unsharp-masked image of the core of 2A 0335+096, using the same smoothing parameters as Fig. 1. (Right) C-band VLA radio map of the same region.

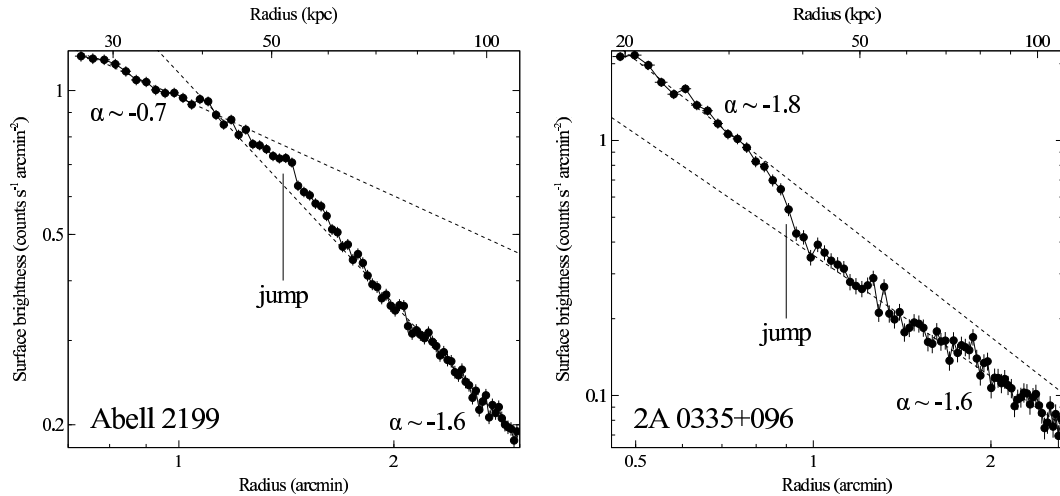


Figure 3. (Left) Surface brightness profile across the discontinuity in Abell 2199 in the 0.5 to 6 keV band. Note the change in slope around 1.4 arcmin. The profile was made between angles 186 and 290 degrees from the north from the west, and was centred on the position $16^h 28^m 38.0^s$, $+39^\circ 33' 24''$ (J2000). (Right) Surface brightness profile for 2A 0335+096. This was made between angles 246 and 351 degrees, and centred on $03^h 38^m 41.3^s$, $+09^\circ 57' 57''$. The plots show powerlaw fits to the inner and outer parts of the profiles.

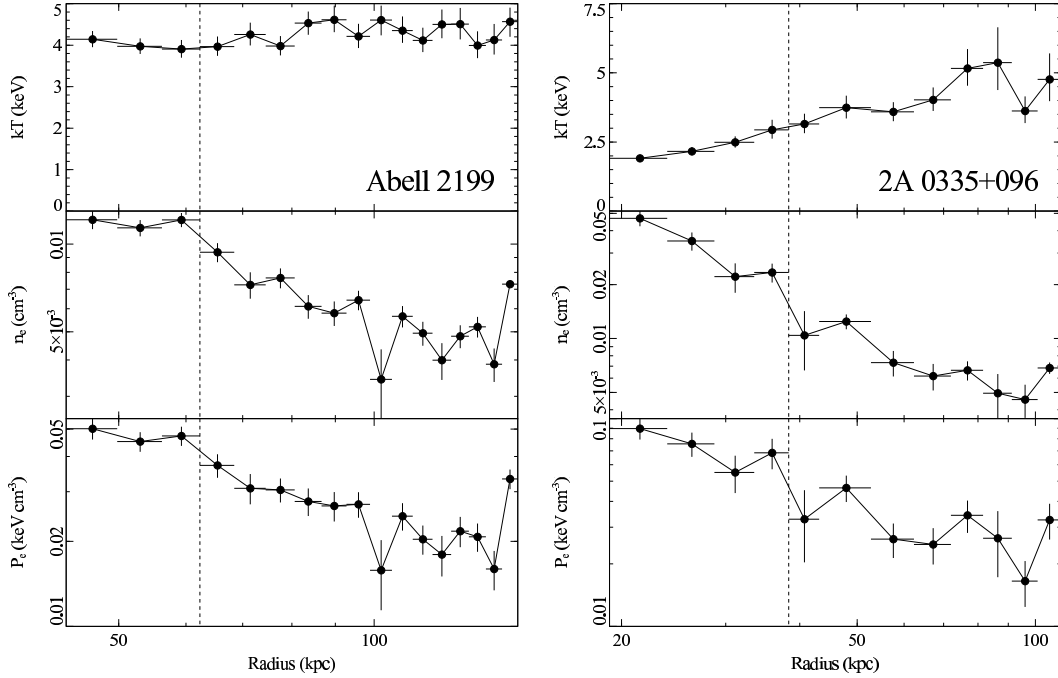


Figure 4. Projected temperature, deprojected density, and pressure across the surface brightness jump in Abell 2199 (left) and 2A 0335+096 (right). The dotted lines show the approximate positions of the surface brightness discontinuities.

make the gas appear isothermal. These include electron-proton coupling, and non-ionization equilibrium. The latter has too short a timescale (less than one million yr) to be relevant, whereas the former takes about 2×10^7 yr. However compression of both electrons and protons dominates the heating in weak shocks so it is unclear whether it would have a significant effect. The conduction timescale is about $5 \times 10^6 \ell_1^2$ yr, where ℓ_1 is the distance from the shock in units of 10 kpc and Spitzer electron conductivity is assumed. The shock propagation timescale is about 10 Myr per 10 kpc, so if conduction is efficient then it can operate to make the shock appear isothermal. The conclusion on the nature of the shocks is therefore similar to that reached for the Perseus cluster (Fabian et al 2006).

Cosmic rays can also pass through the shock front and so transfer energy from shocked to unshocked gas. The inner regions of cool cores are likely to contain a significant cosmic-ray population (see e.g. the discussion of the Perseus radio mini-halo in Sanders et al 2005). If much of the shock energy passes into the cosmic-rays and magnetic field, rather than into the thermal X-ray emitting population, then the thermal gas can appear to be isothermal. We speculate that the cosmic rays can then release much of the shock energy at later times and over a wider region. This possibility may vary from cluster to cluster depending on the energy density of the cosmic rays in the relevant region.

An alternative possibility is that some features are due to changes in metallicity, rather like the metal-rich ring found in the Perseus cluster (Sanders et al 2005). As reported at the end of Section 3, we find no metallicity jumps which could explain the features on Abell 2199 or 2A 0335+096.

Deeper X-ray observations of these cluster cores are required to understand the nature of the shock-like features further. Both A2199 and 2A 0335+096 have X-ray bright cores (0.7 and 0.5 ct s⁻¹ arcmin⁻², respectively at centre of the jump) and relatively brief current Chandra observations. Exposures which are 5–

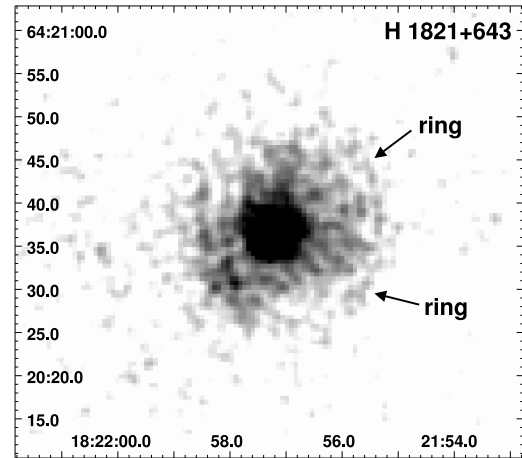


Figure 5. 99.6 ks image of the central region of the cluster around H 1821+643 in the 0.5 to 3 keV band, smoothed with a Gaussian of 0.5 arcsec. This image is the zeroth order LETG image. The dispersion directions lie along SW-NE and SWW-NEE directions. This is *Chandra* OBS.ID 1599.

10 times deeper are feasible and would enable the shape and temperatures of the features to be characterized in detail.

ACKNOWLEDGEMENTS

ACF thanks the Royal Society for support.

REFERENCES

Dunn R.J.H., Fabian A.C., Taylor G.B., 2005, MNRAS, 364, 1343

- Fabian A.C., Sanders J.S., Taylor G.B., Allen S.W., Crawford C.S., Johnstone R.M., Iwasawa K., 2006, MNRAS, 366, 417
Forman W., et al., 2006, in preparation
Giovannini G., Cotton W. D., Feretti L., Lara L., Venturi T., 1998, ApJ, 493, 632
Johnstone R.M., Allen S.W., Fabian A.C., Sanders J.S., 2002, MNRAS, 336, 299
Kawano N., Ohto A., Fukazawa Y., 2003, PASJ, 55, 585
Markevitch M. et al., 2000, ApJ, 541, 542
Markevitch M., 2002, astro-ph/0205333
Mazzotta P., Edge A.C., Markevitch M., 2003, ApJ, 596, 190
Peres C.B., Fabian A.C., Edge A.C., Allen S.W., Johnstone R.M., White D.A., 1998, MNRAS, 298, 416
Sanders J.S., Fabian A.C., Dunn R.J.H., 2005, MNRAS, 360, 133
Sarazin C.L., Baum S.A., O'Dea C., 1995, ApJ, 451, 125
Werner N., de Plaa J., Kaastra J.S., Vink J., Bleeker J.A.M., Tamura T., Peterson J.R., Verbunt F., 2006, A&A, accepted, astro-ph/0512401
Wilson A.S., Smith D.A., Young A.J., 2006, ApJ, in press